Slip Diffusion and Lévy Flights of an Adsorbed Gold Nanocluster

W. D. Luedtke and Uzi Landman

School of Physics, Georgia Institute of Technology, Atlanta, Georgia 30332-0430
(Received 11 January 1999)

Anomalous diffusion of a gold nanocrystal Au_{140}, adsorbed on the basal plane of graphite, exhibiting Lévy-type power-law flight-length and sticking-time distributions, is predicted through extensive molecular dynamics simulations. An atomistic collective slip-diffusion mechanism is proposed and analyzed. [S0031-9007(99)09082-1]

Diffusion processes of atoms, molecules, and clusters on solid surfaces continue to be subjects of active research of basic and technological interest (e.g., in the areas of film growth and catalysis), and a source of discovery pertaining to diffusional energetics and mechanisms [1]. In particular, enhanced diffusion rates of adsorbed small metal clusters containing up to ~10 atoms have been observed in early field-ion microscopy investigations [2(a)] and described using a random walk with internal state formalism [2(b)]. More recently, a dislocation mechanism [3] for surface migration of large two-dimensional clusters and a collective slip-diffusion model for rapid surface diffusion of thiol-passivated gold nanoclusters on graphite [4] have been proposed. Additionally, we note recent experiments [5(a)] and molecular dynamics (MD) simulations [5(b)] pertaining to the rapid diffusion of clusters on solid surfaces. In particular, in Ref. [5(b)] it was concluded, from simulations of large Lennard-Jones clusters on a solid surface, that when the cluster is incommensurate with the substrate fast diffusion occurs via a Brownian-like mechanism.

We report here on a novel surface diffusion phenomenon, where large (hundreds of atoms) three-dimensional gold clusters adsorbed on a graphite surface are predicted via atomistic MD simulations to undergo anomalous diffusive motion with surprisingly high rates, occurring through a collective slip-diffusion mechanism, involving long sliding trajectories, which may be described mathematically as Lévy flights [6].

Normal diffusion is characterized by a variance of the displacements $\sigma^2(t) = \langle [r(t) - r(0)]^2 \rangle \sim t^\gamma$ growing in the long-time limit linearly with t, i.e., $\gamma = 1$. Superdiffusion ($\gamma > 1$) may occur when the trajectories exhibit long displacements (flights), termed "Lévy flights" [6], characterized by power-law (rather than exponential) flight-length (ℓ_F) and flight-time (t_F) probability distribution functions, $P_F(\ell) \sim \ell^{-\mu'}$ and $P_F(t) \sim t^{-\mu}$ ($1 < \mu, \mu' < 3$), which are equivalent (i.e., $\mu = \mu'$) when the flights occur with constant velocity. For such processes the mean-square displacement is divergent with time. Although studied extensively theoretically, physical realizations of Lévy superdiffusion are few and recent, including self-diffusion in polymerlike breakable micelles [6(b),7(a)], tracer transport in turbulent surface waves [7(b)] and

oceanic flow [7(c)], and in chaotic transport studied in a two-dimensional rotating laminar fluid flow [7(d)].

In this paper we focus on the diffusion of a gold nanocrystal (Au_{140}), with a face-centered-cubic structure and a truncated-octahedral morphology adsorbed on the basal plane of graphite (see inset of Fig. 1). The interactions between the gold atoms were described using the embedded-atom potentials [8(a)], those in graphite were modeled following Ref. [8(b)], and for the interaction between the gold and graphite atoms we employed a 6-12 Lennard-Jones potential with the use of combination rules [9]. Simulations were performed for both a static graphite surface and a dynamic one (yielding similar results) and for various temperatures; in the case of canonical simulations, thermalization occurred through scaling of the surface graphite atoms and, in the frozen substrate case, microcanonical (constant energy) simulations were performed following prolonged equilibrations to the desired (kinetic) temperatures. Integration time steps of 3 and 1 fs were used in the static and dynamic surface simulations, respectively, and particularly long simulations were performed to gain statistical significance (the results shown are from a 90 ns simulation at 500 K, and a static graphite surface).

The xy trajectory of the cluster's center of mass (CM) is shown in Fig. 1(a), and its x component is displayed in Fig. 1(b) with two successive tenfold expansions of the time scales; the latter illustrates the self-similar nature of the cluster's diffusive motion, which is a characteristic of Lévy processes [6]. Even a cursory visual inspection of the trajectory shown in Fig. 1 suggests that it may be divided into "free flight" time intervals, and "sticking" intervals when the cluster undergoes localized vibrations. To quantify this observation we use configurations along the dynamic trajectory (separated 1.5 ps apart), and for each (say, the one at time t_i) we examine the distance between the CM position at times $t_i + \tau/2$ and $t_i - \tau/2$ (where τ is equal to half the lateral vibrational period of the CM during a sticking interval; at 500 K, $\tau \simeq 20$ ps), i.e., $d(t_i) = |\mathbf{R}(t_i + \tau/2) - \mathbf{R}(t_i - \tau/2)|$. A histogram of $d(t_i)$ is shown in the inset (i) of Fig. 2, exhibiting a bimodal character, with the narrow peak for $d \leq 0.6$ Å corresponding to vibrational motions (assigned as sticking
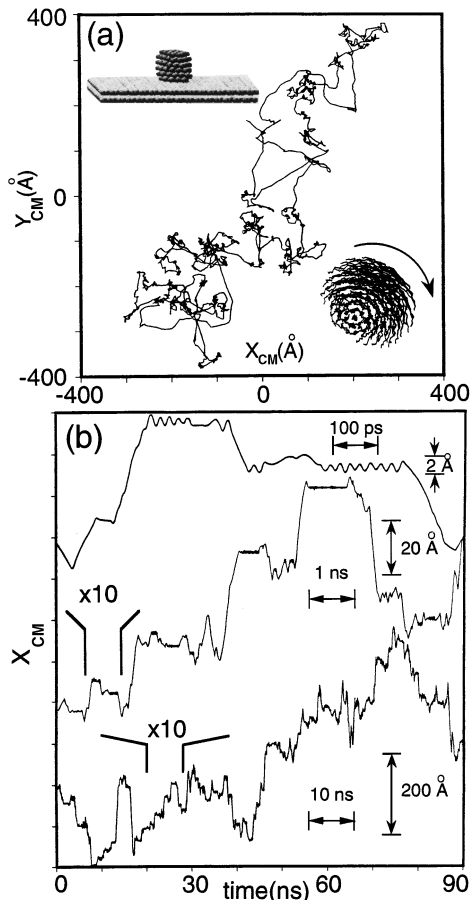
FIG. 1. (a) A 90 ns (xy) trajectory of the center of mass (CM) of a Au_{140} cluster diffusing on the basal plane of graphite at 500 K (x and y in units of Å). Insets: top left: atomic configuration of the adsorbed cluster on the surface; bottom right: a top view of a short-time trajectory of the cluster illustrating pivotal-slip motion. (b) X_{CM} vs time. For the bottom curve, the time span is 90 ns and the coordinate (X_{CM}) as indicated. The upper two curves correspond to two successive tenfold expansions of the time scale of the indicated intervals. The corresponding changes in the coordinate scales are as indicated.

FIG. 2. Flight [P_F, in (a)] and sticking [P_S, in (b)] probability distributions, exhibiting power-law decay with exponents $\mu = 2.3$ and $\nu = 2.1$, respectively. Statistical uncertainty in the data, related to the analysis leading to the classification of flight and sticking intervals, is estimated to be smaller than the size of the dots. The quality of the straight line fits to the data, measured by the root-mean-square (rms) deviations are 0.06 and 0.04 in (a) and (b), respectively. Attempting to fit the data by an exponential law resulted in significantly inferior fits [rms deviations of 0.17 and 0.24 for (a) and (b), respectively]. Insets: (i) histogram of the beginning-to-end length (d) of flights calculated for time intervals ($t_i - \tau/2$, $t_i + \tau/2$) vs d (in Å); (ii) scatter plot of the flights' lengths (d_F, in Å) plotted vs the (discrete) flights' durations (t_F; in ns); (iii) log-log plot of the variance of the gold cluster CM displacement [$\langle R^2(t) \rangle$ in cm^2, averaged over time origins] vs time. The dashed line indicates the slope at the long-time limit.

configurations) and the broad distribution for $d > 0.6$ Å corresponding to nonoscillatory displacements (assigned as flights). A contiguous set of sticking configurations comprises a sticking interval, and similarly we define a flight interval. Consequently, the total trajectory is divided into a succession of sticking and flight intervals; note that a segment where the 2D trajectory changes direction abruptly (large curvature) is likely to be classified as a sticking one since, during the time $\pm \tau/2$, the CM tends to remain localized.

Prior to addressing the Lévy character of the motion of the cluster on the surface we use the above classification and show in Fig. 2 [inset (ii)] a scatter plot of the path lengths (d_F), calculated along the flight's trajectory, plotted (for each flight) against the flight's duration (t_F). We observe some dispersion in this plot corresponding to a
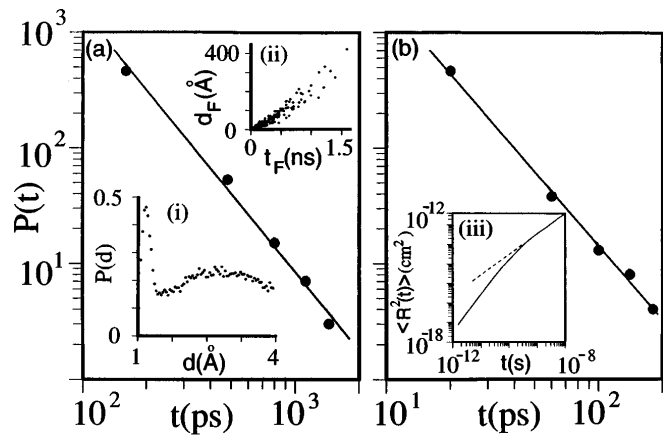
distribution of flight speeds about a mean value of 15 m/s [10]. This observation, as well as some variation of the cluster CM velocity during individual flights (indicating deviations from pure ballistic behavior), is of relevance to the formulation of certain theoretical models of Lévy processes [in particular, constant and nonconstant velocity models, see Refs. [11(a)] and [11(b)].

To test for a Lévy character of the diffusion we display in Figs. 2(a) and 2(b) the flight (P_F) and sticking (P_S) probability distributions which indicate $P_F(t) \sim t^{-\mu}$ with $\mu \sim 2.3$, and $P_S(t) \sim t^{-\nu}$ with $\nu \approx 2.1$. Additionally, we show in Fig. 2 [inset (iii)] a plot of $\log R^2(t)$ vs $\log(t)$, where $R^2(t) = \langle [\mathbf{R}(t) - \mathbf{R}(0)]^2 \rangle$ with $\mathbf{R}$ the CM position and the angle brackets denoting averaging over time origins. The slope of the curve at large t equals 1.1, i.e., $R^2(t) \sim t^{1.1}$, that is, indicating mild superdiffusion of the cluster at $T = 500$ K.

In light of the coexistence of flights and sticking events found in the above simulations, we note that several studies, pertaining to the connection between Lévy-type motion and the character of the ensuing diffusion (that is, the exponent γ), have shown [11(a)] and [11(b)] that the interplay between the flight and sticking exponents (μ and ν, respectively) can lead to crossovers between the various diffusion regimes (i.e., regular with $\gamma = 1$ and anomalous with $\gamma \neq 1$). Using our values for μ and ν in

relations obtained from these theories leads indeed to estimated values [11(c)] of $\gamma > 1$.

To further explore the atomistic origins of the Lévy flight character of the diffusion process observed in our simulations, we plot in Fig. 3 a segment of the trajectory [see Fig. 1(b)] along with the corresponding variation in the cluster-to-surface (CS) interaction energy (E_{CS}) and the cluster's CM distance Z_{CM} from the surface plane. It is evident that the behavior of E_{CS} and Z_{CM} are essentially identical, and that both correlate strongly with sticking and flight intervals (that is, both decrease during sticking). These correlations suggest that the high mobility of the cluster on the surface originates from its interfacial incommensurability. The situation may be illustrated by placing a finite planar raft made of spheres of a certain intersphere distance over an extended one characterized by a different intersphere distance, and allowing for interaction between the spheres of the two rafts. Under such circumstances, certain relative configurations of the two rafts will result in an improved "tight fit" between them characterized by a smaller interraft distance and stronger interaction (such configurations correspond to sticking intervals). However, for the large majority of relative interraft configurations only a "loose fit" can be achieved resulting in a larger interraft interfacial separation and a
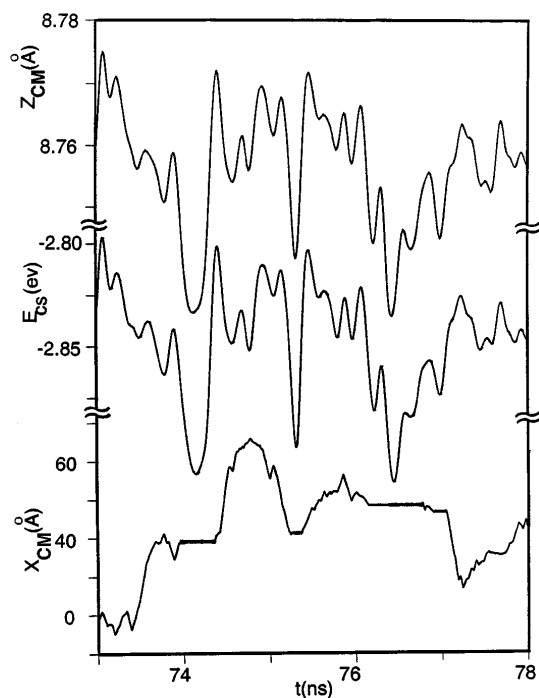

FIG. 3.　Bottom: the cluster CM x coordinate (X_{CM}) vs time (in ns) during a segment of it's motion [$73 \le t \le 78$ ns, see bottom curve in Fig. 1(b)]. Middle and top: the cluster-to-surface interaction energy (E_{CS}, middle, in eV) and CM z coordinates (Z_{CM}, top, in Å) during the same time interval. Note the drops in E_{SC} and Z_{CM}, correlated with sticking intervals. The E_{CS} and Z_{CM} curves were obtained through Gaussian smoothing of the MD data, with a width of 90 ps.

weaker interaction. Consequently, starting from a sticking configuration, once the (fluctuating) distribution of energy between the various degrees of freedom of the cluster concentrates sufficient energy into the CM lateral motions the cluster may overcome the barrier for transition into a nonsticking configuration characterized by weaker coupling to the surface. Since the probability for finding another sticking configuration is small (due to their infrequency and small configurational "catchment" basins), the cluster will continue to displace ("fly") for an extended distance, till it will be trapped again [12].

The above diffusion mechanism is a cooperative one and may be termed [4] "slip diffusion" (SD), accompanied by occasional "pivoted slips" [see lower inset of Fig. 1(a)]. To first approximation the initiation of diffusive motion in this mechanism may be described using a simple model [4]. The occurrence of slip requires that the effective lateral shear stress $\sigma_\parallel$, associated with thermal vibrations of the cluster CM (i.e., lateral restoring force on the cluster divided by the contact area S between it and the graphite surface), exceeds a critical value. From simulations at low temperature, we determined effective CM spring constants for lateral ($k_\parallel = 0.08$ mdyn/Å) and vertical ($k_\perp = 1.5$ mdyn/Å) vibrations (with vibrational periods of $\tau_\parallel = 15$ ps and $\tau_\perp = 3.5$ ps), respectively. This leads to an estimate of the maximum lateral vibrational restoring stress $\sigma_{\parallel m} = (2k_\parallel k_B T)^{1/2}/S$, where k_B is the Boltzmann constant. The critical lateral shear stress for slip, σ_c, was determined in a separate simulation by applying to the adsorbed cluster (in a stuck configuration) a progressively increasing uniform force until slip was initiated, yielding $\sigma_c \simeq 245$ Mpa. (In obtaining this estimate, we consider only pure translational motion of the cluster CM. Consequently, the estimated value of σ_c is an upper bound for the initiation of slip [13].) The increase in E_{CS} accompanying the initiation of slip in this calculation was ~ 0.1 eV (compare also with Fig. 3, where a similar change in E_{CS} is found from the MD simulation). From $\sigma_{\parallel m} = \sigma_c$ with $S = 130$ Å^2, the temperature T_S, at which significant slip could be initiated, may be estimated, yielding $T_S = 500$ K (for the thiol-passivated cluster a much lower value was determined [4], $T_S = 80$ K). Below the temperature T_S the clusters display slip but much less frequently and T_S, in analogy with conventional descriptions of diffusion, may be interpreted as the temperature for which the thermal energy of the diffusing entity equals or exceeds the energy barrier [13] for motion between neighboring potential wells. These simple estimates for initiating enhanced slip diffusional motion, with a significant reduction in sticking events, agree with our observations of the temperatures for which enhanced surface mobility of the clusters occurred.

In conclusion, we remark that the anomalous diffusion characterized by Lévy-type power-law distributions for the flight and sticking events, predicted by our MD simulations, and the estimates obtained through our cooperative

slip-diffusion model are likely to depend on the temperature, degree of commensurability between the adsorbate and the surface, and on the coupling strength between them. These issues, as well as effects due to surface imperfections [14], are challenges for further experimental and theoretical studies.

[1] See *NATO-ASI Surface Diffusion: Atomistic and Collective Processes,* edited by M. C. Tringides (Plenum, New York, 1997); see also S. C. Wang, U. Kurpick, and G. Ehrlich, Phys. Rev. Lett. **81**, 4923 (1998), and references therein.

[2] (a) K. Stolt, W. R. Graham, and G. Ehrlich, J. Chem. Phys. **65**, 3206 (1976); (b) U. Landman, E. W. Montroll, and M. F. Shlesinger, Phys. Rev. Lett. **38**, 285 (1977), and references to early experiments cited therein.

[3] J. C. Hamilton, M. C. Daw, and S. M. Foiles, Phys. Rev. Lett. **74**, 2760 (1995); U. Landman and W. D. Luedtke, Appl. Surf. Sci. **92**, 237 (1996).

[4] W. D. Luedtke and U. Landman, J. Phys. Chem. **100**, 13 323 (1996).

[5] (a) L. Bardotti *et al.,* Surf. Sci. **367**, 276 (1996); (b) P. Deltour, J.-L. Barrat, and P. Jensen, Phys. Rev. Lett. **78**, 4597 (1997).

[6] (a) See articles in *Lévy Flights and Related Topics in Physics,* edited by M. F. Shlesinger, G. M. Zaslavsky, and U. Frisch (Springer, Berlin, 1995); (b) J.-P. Bouchaud and A. Georges, Phys. Rep. **4-5**, 127 (1990).

[7] (a) J. P. Bouchaud *et al.,* J. Phys. II (France) **1**, 1465 (1991); (b) R. Ramshankar and J. P. Gollub, Phys. Fluids A **3**, 1344 (1991); (c) M. G. Brown and K. B. Smith, Phys. Fluids A **3**, 1186 (1991); A. R. Osborne *et al.,* Tellus **41A**, 416 (1989); (d) T. H. Solomon, E. R. Weeks, and H. Swinney, Phys. Rev. Lett. **71**, 3975 (1993).

[8] (a) The parametrization used is after J. B. Adams, S. M. Foiles, and W. G. Wolfer, J. Mater. Res. **4**, 102 (1989); C. L. Cleveland *et al.,* Phys. Rev. Lett. **79**, 1873 (1997). (b) F. F. Abraham and I. P. Batra, Surf. Sci. Lett. **209**, L125 (1989).

[9] For the LJ potential well depth and distance parameters, we used $\varepsilon(\text{Au-C}) = 0.01273$ eV and $\sigma(\text{Au-C}) = 2.9943$ Å (see also Ref. [4]).

[10] The distribution of the flights' speeds obtained from the data in inset (ii) of Fig. 2 is close to a Gaussian with a mean flight speed of $\bar{\nu}_F = 15$ m/s and a FWHM of 12 m/s, compared to a $\bar{\nu}_F = 15$ m/s and a larger FWHM of 20 m/s for a Maxwell-Boltzmann distribution at 500 K.

[11] (a) J. Klafter, G. Zumofen, and M. F. Shlesinger, in Ref. [6(a)], p. 196; (b) G. M. Zaslavsky, *ibid.,* p. 216; (c) see Eq. (37) in Ref. [11(a)] and Eq. (2.9) in Ref. [11(b)]. Further quantitative comparison between the simulation results and these theoretical studies are not warranted in light of the models' assumptions.

[12] Since the laws of Brownian motion (normal diffusion) result from the central limit theorem (CLT) of probability theory, one may look for the origins of "anomalous" diffusion phenomena, such as the one discussed here, in the failure of the conditions leading to the CLT [6(b)]. Such failure may result from (i) a broad distribution of the diffusion jump lengths (as measured through the behavior of the second moment of the distribution) and/or (ii) long range correlations between them. The physical picture described above, pertaining to the atomistic origins of the long flights observed in our simulations, relates particularly to condition (i). Further studies of this issue are currently in progress.

[13] In the context of our discussion of the transition between sticking and flight intervals, we note that the cluster's internal and rotational (pivotal and wagging) degrees of freedom act as sources and sinks (reservoirs) for the exchange of energy with the cluster's CM translational degrees of freedom. Additionally, during a sticking configuration, pivotal rotational motions cause misalignments at the cluster-to-surface interface, accompanied by decreased binding to the surface. As a result of such processes the barriers for slip may be decreased and initiation of slip motion may occur by surmounting a smaller effective energy barrier. This scenario is consistent with our observation that just prior to slip events the cluster's degree of commensurability with the surface, as measured by E_{CS} and Z_{CM} (see Fig. 3), has often already undergone a significant change.

[14] Because of the predicted high surface mobility of the adsorbed clusters, they are likely to be found primarily at pinning sites, such as steps and surface defects, or as part of cluster islands.